Journal of Cerebral Blood Flow & Metabolism (2013) 33, 708–715

www.jcbfm.com

ORIGINAL ARTICLE

Induction of hyperhomocysteinemia models vascular dementia by induction of cerebral microhemorrhages and neuroinflammation

Tiffany L Sudduth[1], David K Powell[2,3], Charles D Smith[2,4], Abigail Greenstein[1] and Donna M Wilcock[1]

Vascular dementia (VaD) is the second leading cause of dementia behind Alzheimer's disease (AD) and is a frequent comorbidity with AD, estimated to occur in as many as 40% of AD patients. The causes of VaD are varied and include chronic cerebral hypoperfusion, microhemorrhages, hemorrhagic infarcts, or ischemic infarcts. We have developed a model of VaD by inducing hyperhomocysteinemia (HHcy) in wild-type mice. By placing wild-type mice on a diet deficient in folate, B6, and B12 and supplemented with excess methionine, we induced a moderate HHcy (plasma level homocysteine 82.93 ± 3.561 μmol). After 11 weeks on the diet, the hyperhomocysteinemic mice showed a spatial memory deficit as assessed by the 2-day radial-arm water maze. Also, magnetic resonance imaging and subsequent histology revealed significant microhemorrhage occurrence. We found neuroinflammation induced in the hyperhomocysteinemic mice as determined by elevated interleukin (IL)-1β, tumor necrosis factor (TNF)α, and IL-6 in brain tissue. Finally, we found increased expression and increased activity of the matrix metalloproteinase 2 (MMP2) and MMP9 systems that are heavily implicated in the pathogenesis of cerebral hemorrhage. Overall, we have developed a dietary model of VaD that will be valuable for studying the pathophysiology of VaD and also for studying the comorbidity of VaD with other dementias and other neurodegenerative disorders.

Journal of Cerebral Blood Flow & Metabolism (2013) **33,** 708–715; doi:10.1038/jcbfm.2013.1; published online 30 January 2013

Keywords: animal models; hemosiderin; homocysteinemia; inflammation; vascular dementia

INTRODUCTION

Vascular dementia (VaD) is defined as the loss of cognitive function to a degree that interferes with activities of daily living, resulting from ischemic or hemorrhagic cerebrovascular disease or from cardiovascular or circulatory disturbances that injure brains regions important for memory, cognition, and behavior.[1] It is the second most common form of dementia after Alzheimer's disease (AD), accounting for 20% of all dementia cases worldwide.[2] In addition, however, VaD is thought to occur in 20% to 55% of AD cases.[3] In the Religious Orders Study, 39% of autopsy-proven AD subjects also had macroscopic brain infarcts.[4] The comorbidity of VaD and AD in a significant number of cases likely prevents a clear therapeutic effect from being observed in the numerous clinical trials for late-onset AD that have been pursued to date.

Vascular dementia describes a collective group of dementias caused by cerebrovascular disease. This can encompass hemorrhagic or ischemic events, white-matter or gray-matter lesions, and systemic cardiovascular events leading to central hypoperfusion or central cerebrovascular issues themselves.[5] The diversity in conditions that can cause a dementia, and that are named 'vascular dementias', has complicated the study of VaD. There is no single pathology to be studied or one single mutation known to result in VaD. To begin to study VaD, we have elected to study the form of VaD attributed to the presence of multiple microhemorrhages in the cerebral cortex. Hyperhomocysteinemia (HHcy) is considered to be an independent risk factor for cardiovascular disease and stroke. In addition, it is now considered to be a risk factor for several neurodegenerative diseases including AD and VaD. It can result from deficiencies of vitamins B6 (pyridoxine), B9 (folic acid), or B12. Homocystinuria and HHcy caused by inborn defects in cystathionine-β-synthase is a recognized cause of stroke in children and young adults.[6] Previous studies inducing HHcy in rodent models have shown that it results in cognitive decline,[7] systemic vascular inflammation, atherosclerosis,[8] and a loss of central cholinergic neurons.[9]

Relative to AD, VaD has been relatively understudied with respect to animal models, pathophysiology, and identification of distinct therapeutic targets. Our goal in the current study was to test the hypothesis that dietary induction of HHcy in wild-type mice models a form of VaD caused by multiple microhemorrhages and neuroinflammation.

MATERIALS AND METHODS

Animals

Twenty C57BL6 wild-type mice aged 3 months were randomly assigned to one of two groups. One group was placed on diet with low levels of folate, vitamins B6, and B12 and enriched with methionine ($N = 15$ for behavioral outcomes; 10 for all other outcome measures shown) (Harlan Teklad TD97345; Harlan Teklad, Madison, WI, USA), while the another group was placed on a control diet that nutritionally matched the experimental diet with normal levels of methionine, folate, and vitamins B6 and B12 ($N = 15$ for behavioral outcomes; 10 for all other outcome measures shown) (Harlan Teklad 5001C; Harlan Teklad). Mice received diet for 14 weeks. Mice were weighed weekly to ensure no significant malnourishment was

[1]Department of Physiology, Sanders-Brown Center on Aging, University of Kentucky, Lexington, Kentucky, USA; [2]Magnetic Resonance Imaging and Spectroscopy Center, Sanders-Brown Center on Aging, University of Kentucky, Lexington, Kentucky, USA; [3]Department of Biomedical Engineering, Sanders-Brown Center on Aging, University of Kentucky, Lexington, Kentucky, USA and [4]Department of Neurology, Sanders-Brown Center on Aging, University of Kentucky, Lexington, Kentucky, USA. Correspondence: Dr DM Wilcock, Sanders-Brown Center on Aging, University of Kentucky, 800 South Limestone Street, Lexington, KY 40536, USA.
E-mail: donna.wilcock@uky.edu
This work was funded by NIH grant NS079637 (DMW).
Received 22 October 2012; revised 10 December 2012; accepted 28 December 2012; published online 30 January 2013

occurred because of the diet. The study was approved by the University of Kentucky Institutional Animal Care and Use Committee and conformed to the National Institutes of Health Guide for the Care and Use of Animals in Research.

Behavior Testing

Radial-arm water maze testing and rotarod testing were performed in a blinded manner by the University of Kentucky Rodent Behavior Core (http://www.rodentbehaviorcore.uky.edu/). Behavior testing was performed in the 6 days before tissue harvest.

For the rotarod (San Diego Instruments Inc., San Diego, CA, USA), mice were initially placed on the stationary drum and the drum was started at the lowest speed (4 r.p.m.), accelerating over time until the mouse fell off into the catch area. A photo beam accurately measured the mouse for fall to assess time to latency. The mice were subjected to three training sessions lasting 1 minute each with 10 minutes between each session. There was a wait time of 30 minutes between training and the test sessions. For the test sessions, the rotating drum was set to accelerate from 0 to 40 r.p.m. over 5 minutes. There were two test sessions with 15 minutes between each test session. After all the sessions in a single day were completed, the mouse was returned to its home cage. The training and test sessions were repeated for 4 consecutive days. We measured the average distance traveled for the two test trials on each of the 4 days.

The 2-day radial-arm water maze protocol was performed as previously published.[10] Briefly, a six-arm maze was submerged in a pool of water, and a platform was placed at the end of one arm (equipment and tracking software from Noldus Information Technology Inc., Leesburg, VA, USA). Each mouse received 15 trials per day for 2 days. The mouse began each trial in a different arm while the arm containing the platform remained the same. The numbers of errors (incorrect arm entries) were counted over a 1-minute period. The errors were averaged over 3 trials, resulting in 10 blocks for the 2-day period (blocks 1 to 5 are day 1 while blocks 6 to 10 are day 2).

Magnetic Resonance Imaging

A subset of study mice were imaged by T2* magnetic resonance imaging (MRI). Three mice receiving control diet and four mice receiving experimental diet were imaged immediately before kill using the T2* MRI technique to assess the microhemorrhage incidence. The imaging staff was blinded to the experimental groups. Mice were imaged using a 7-T Bruker ClinScan MRI system (Bruker, Billerica, MA, USA) with an MRI CyroProbe, delivering 2.5 times the signal to noise of a standard room temperature radiofrequency coil, located at the Magnetic Resonance Imaging and Spectroscopy Center at the University of Kentucky. Fourteen coronal slices were acquired with a FLASH sequence with a repetition time of 165 ms, echo time 15.3 ms, 25° flip angle, 448×448 matrix, 0.4 mm thick, 20% gap, 0.033 mm $\times$ 0.033 mm resolution, 10 averages, and acquisition time 24 minutes. Mice were anesthetized with 1.3% isoflorane in oxygen using an MRI compatible vaporizer. They were then positioned prone and held in place on the scanning bed using tooth and ear bars. The animals were maintained at 37°C with a water heated scanning bed. Body temperature, heart, and respiration rates were monitored. The T2* MRI images were analyzed by two blinded investigators who identified abnormalities that resembled hemorrhagic infarcts. These infarcts were counted and this number was normalized to the number of images counted to provide a per section count.

Tissue Processing and Histology

After injection with a lethal dose of pentobarbital, blood was collected for plasma and the mice were perfused intracardially with 25 mL normal saline. Brains were rapidly removed and bisected in the mid-sagittal plane. The left half was immersion fixed in 4% paraformaldehyde for 24 hours, while the right half was dissected into anterior cerebral cortex, posterior cerebral cortex, striatum, hippocampus, thalamus, cerebellum, and rest of brain. The posterior cerebral cortex and rest of brain were combined and immediately homogenized in phosphate-buffered saline for zymography (see detailed method below). The remaining pieces were flash frozen in liquid nitrogen and stored at -80°C. The left hemibrain was passed through a series of 10%, 20%, and 30% sucrose solutions as cryoprotection and 25 μm frozen horizontal sections were collected serially using a sliding microtome and stored floating in phosphate-buffered saline containing sodium azide at 4°C. Plasma was analyzed in a blinded manner by a veterinary reference diagnostics service for lipid and homocysteine levels (see Table 1; Antech Diagnostics, Fishers, IN, USA).

Eight sections equally spaced 600 mm apart were selected for free-floating immunohistochemistry for CD11b (Rat monoclonal, AbD Serotec, Raleigh, NC, USA; 1:3,000). The method for free-floating immunohistochemistry has been described previously.[11] Sixteen sections equally spaced 300 mm apart were mounted on slides and stained for Prussian blue as described previously.[12] Immunohistochemical analysis was performed by measuring percent area occupied by positive stain using the Nikon Elements BR image analysis system (Melville, NY, USA) as described previously.[13] The experimenter was blinded to the group assignments.

Quantitative Real-Time RT-PCR

RNA was extracted from the frozen right hippocampus using the Trizol plus RNA purification system (Life Technologies, Grand Island, NY, USA) according to manufacturer's instructions. RNA was quantified using the nanodrop spectrophotometer (Thermo Scientific, Rockford, IL, USA) and cDNA produced using the cDNA High Capacity kit (Life Technologies) according to manufacturer's instructions. Real-time PCR was performed using the TaqMan Gene Expression assay kit (Life Technologies) according to manufacturer's instructions and as previously described.[14] The genes examined are summarized in Supplementary Table; all were normalized to 18S rRNA. We determined fold change for mice receiving the experimental diet compared with mice receiving the control diet using the $^{-\Delta\Delta Ct)}$ method.[15]

ELISA Measurement

Protein was extracted from the right frontal cortex in phosphate-buffered saline with complete protease and phosphatase inhibitor (Pierce Biotechnology Inc., Rockford, IL, USA) and quantified using the BCA protein assay kit (Pierce Biotechnology Inc., performed according to manufacturer's instructions). We used commercially available kits to assess matrix metalloproteinase 2 (MMP2), tissue inhibitor of metalloproteinase 2 (TIMP2), MMP9, and TIMP1, and ran the assays according to manufacturer's recommendations (R&D Systems, Minneapolis, MN, USA). All data were normalized to the total protein to yield ng/mg protein. Plasma was analyzed for total Factor X and thrombin using commercially available ELISA kits run according to manufacturer's instructions (Molecular Innovations, Novi, MI, USA).

Gelatin Zymography

Enzymatic activities of tissue MMPs were measured using gelatin zymography in brain samples. Protein was extracted from fresh brain tissue in phosphate-buffered saline; specifically right posterior cerebral cortex and rest of brain, and quantified immediately using the BCA protein assay kit (Pierce Biotechnology Inc.; performed according to manufacturer's instructions). Protein samples were immediately separated on a precast 10% gelatin zymogram gel (Life Technologies). The gel was removed, incubated in zymogram renaturing buffer for 30 minutes, equilibrated for 30 minutes in zymogram developing buffer at room temperature and then incubated overnight at 37°C with gently agitation in fresh zymogram developing buffer (all buffers obtained from Life Technologies). The next day, the gel was washed gently with water and incubated in IRDye blue protein stain, a Coomassie stain (Licor, Lincoln, NE, USA). The gel was stained for 1 hour and then destained in H_2O until clear band resolution was apparent ($\sim$1 hour). The gel was imaged on the Odyssey imager and semiquantitative densitometry analysis on our bands of interest was performed using the Odyssey Imaging Software (Licor).

Analysis

Data are presented as mean $\pm$ standard error of mean (s.e.m.). Statistical analysis was performed using the JMP statistical analysis program (SAS, Cary, NC, USA). Radial-arm water maze data and rotarod were analyzed by repeated-measures ANOVA to assess the overall effect of diet. For the radial-arm water maze data, we also performed Student's *t*-test on individual block data. For other data, one-way ANOVA and Student's *t*-test were performed. Statistical significance was assigned where the *P* value was lower than 0.05. Correlations were assessed using the simple linear regression and assessing the R^2 correlation coefficient.

RESULTS

Plasma analysis showed that our diet with low levels of folate, B6, and B12 with enriched methionine did induce a moderate HHcy

Table 1. Plasma analysis of study animals

Analyte	*Control diet*	*Experimental diet*	P-*value*
Homocysteine	**5.89 ± 0.385 μmol/L**	**82.93 ± 3.561 μmol/L**	**<0.0001**
HDL-1	74.26 ± 3.22%	77.34 ± 1.76%	0.39
LDL	9.68 ± 2.13%	8.03 ± 0.62%	0.43
VLDL	13.84 ± 1.99%	13.85 ± 1.66%	0.99
Total Factor X	11.4 ± 1.2 μg/mL	12.1 ± 2.2 μg/mL	0.79
Prothrombin	235 ± 24 ng/mL	212 ± 18 ng/mL	0.87

Abbreviations: HDL-1, high-density lipoprotein 1; LDL, low-density lipoprotein; VLDL, very low-density lipoprotein. The analytes that were statistically significantly different between our control group and our experimental group are shown in bold.

(Table 1). In C57BL6 mice, normal homocysteine levels are considered to be 5 to 12 μmol/L. Hyperhomocysteinemia can be categorized as mild (12 to 30 μmol/L), moderate (30 to 100 μmol/L), and severe (>100 μmol/L).[16] Based on the levels observed in our experimental mice, we achieved a moderate HHcy. None of our mice reached the plasma level of homocysteine to be classified as severe HHcy. We found no change in lipoprotein levels as assessed by the measurement of high-density lipoprotein 1, low-density lipoprotein, and very low-density lipoprotein (Table 1). In addition, analysis of plasma for total Factor X and prothrombin showed that HHCy does not significantly alter the levels of these clotting factors (Table 1).

The 2-day radial-arm water maze task assesses spatial memory performance by measuring the number of incorrect arm entries made in a trial.[10] Over the 2 days of testing the mice receiving control diet show learning of the task, beginning with an average of five errors in block 1 of day 1 and ending with <1 error in block 10 of day 2 (Figure 1A). The HHcy mice were significantly impaired in the radial-arm water maze compared with the control mice, starting with the same number of errors in block one of day 1 but only ending with three errors in block 10 of day 2 (Figure 1A). The rotarod assesses motor function in mice and both the control and HHcy mice performed this task well and were not distinguishable from one another (Figure 1B), suggesting that the HHcy effect in the radial-arm water maze was not because of a motor impairment.

To determine the cerebrovascular pathology induced by the HHcy condition, we performed T2* MRI on three control mice and four HHcy mice. We found significant microhemorrhage-like infarcts as indicated by the arrows in Figure 2A and 2B. To confirm our findings, we performed a Prussian blue histologic stain to detect hemosiderin on all mice from the study. We found a significant increase in microhemorrhage incidence in the HHcy mice compared with the control mice. In addition, we were able to histologically confirm many of the microhemorrhages that had been detected by MRI (Figure 2C and D are the microhemorrhages shown in A and B, respectively, panels E and F show higher magnification images of C and D). The location of microhemorrhages varied greatly; however, we observed a greater frequency of microhemorrhages in the entorhinal and parietal cortices than in the frontal cortex or hippocampal regions. Quantification of microhemorrhage events detected by Prussian blue histology (all animals) and T2* MRI (a subset of animals) is shown in Figure 2G. While T2* MRI detects a significantly fewer number of microhemorrhages than Prussian blue does, the MRI data did correlate strongly with the Prussian blue data (Figure 2H, $R^2 = 0.95$).

Microglial activation is an indicator of neuroinflammation. CD11b is a marker of all microglia in mouse brain and its expression increases in intensity as microglia become activated. We observed increased CD11b staining throughout the brain. This was most noticeable in the cerebral cortex and hippocampal regions (Figures 3A–3H). We found that control cerebral cortex (Figures 3A and 3B) and hippocampus (Figures 3E and 3F) showed

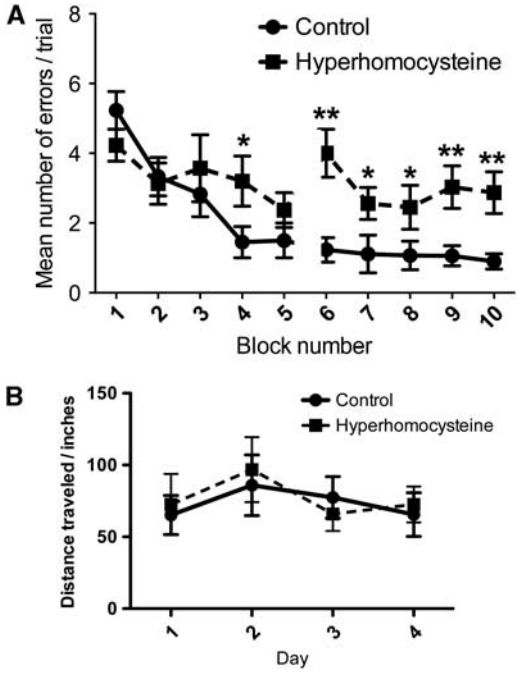

Figure 1. Hyperhomocysteinemia (HHCy) is associated with impaired spatial memory as detected using the radial-arm water maze but does not cause motor deficits. (**A**) Two-day radial-arm water maze data shown as mean number of errors made per trial. Data are given as block numbers; each block represents the average of three trials. **Indicates $P<0.01$ by individual block *t*-test. Also, repeated-measures ANOVA gave a $P<0.01$ for overall group difference in the task. (**B**)The mean distance traveled on the rotarod of the two test sessions for each of the 4 days is shown. For both panels, the closed circles connected by a solid line indicate the mice receiving control diet ($N=15$) and the closed squares connected by the dashed line indicate the mice receiving the experimental diet ($N=15$).

a normal staining pattern for CD11b, with lots of lightly stained microglia populating the brain regions. In our HHcy mice, we found significantly increased CD11b staining in both the frontal cortex (Figures 3C and 3D) and hippocampus (Figures 3G and 3H). Quantitative analysis of the area occupied by positive immunostaining showed significantly increased CD11b staining in all brain regions measured (frontal cortex, CA1, and dentate gyrus of hippocampus and entorhinal cortex) of the HHcy mice compared with our control mice (Figure 3I).

To further examine the neuroinflammatory state of our HHcy mice, we performed qRT-PCR for genes associated with M1 and M2 neuroinflammatory phenotypes. Figure 4A shows gene expression analysis of M1 neuroinflammatory markers interleukin (IL)-1β, IL-6, IL-12, and tumor necrosis factor (TNF)α. All of these M1 markers show significantly increased expression in the HHcy mice

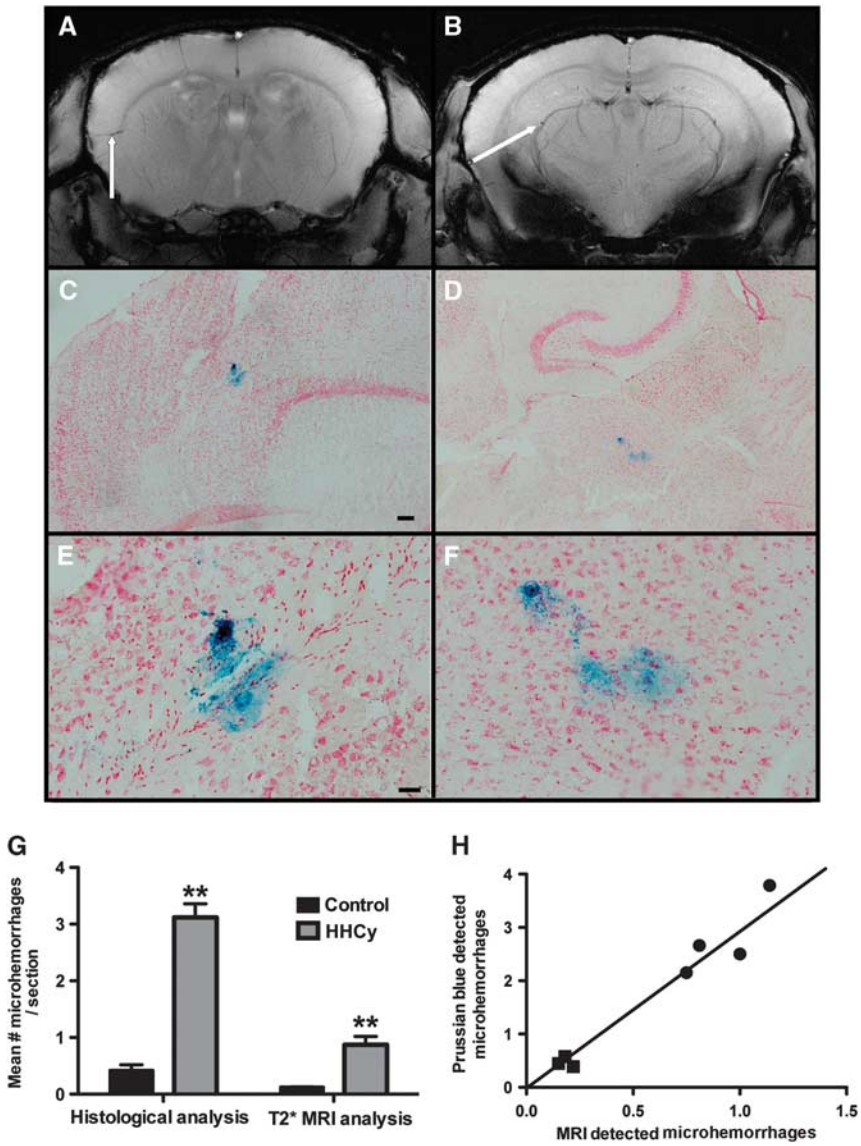

Figure 2. Hyperhomocysteinemia (HHCy) is associated with increased microhemorrhages. (**A**, **B**) Representative coronal T2* MRI images from HHcy mice are shown. The white arrows indicate microhemorrhages. (**C–F**) The Prussian blue-stained horizontal tissue sections are shown. (**C**) The microhemorrhage detected in (**A**), and (**D**) the microhemorrhage detected in (**B**) are shown. (**E**, **F**) High magnification images of (**C**) and (**D**), respectively, are shown. (**C**, **D**) Magnification = $\times$ 40, scale bar in (**C**) for (**C**) and (**D**) = 120 μm; (**E**, **F**) magnification = $\times$ 200, scale bar in (**E**) for (**E**) and (**F**) = 25 μm. (**G**) Quantification of microhemorrhages is shown. Numbers of microhemorrhages were counted and are shown as a per section count for histologic analysis (Prussian blue) in all study animals and for the T2* MRI analysis, which was performed in a subset of animals. **Indicates $P<0.01$ by *t*-test. (**H**) The correlation of MRI detection of microhemorrhages (x axis) and the Prussian blue detection of microhemorrhages (y axis) is shown. Square symbols represent the mice receiving control diet and round symbols represent the mice receiving hyperhomocysteinemic diet. The line shows the line of best fit. R^2 for the correlation = 0.95, $P<0.001$ by linear regression analysis. MRI, magnetic resonance imaging.

compared with our control mice. In contrast, gene expression analysis of M2 neuroinflammatory markers arginase 1, IL-10, IL-1 receptor antagonist , and YM1 do not show significant differences between the HHcy mice and the control mice (Figure 4B).

Components of the MMP2 system are increased in the HHcy mice compared with control mice (Figures 5A and 5B). Gene expression analysis of MMP14, MMP2, and TIMP2 showed significant increases in the HHcy mice compared with control mice (Figure 5A). When we measured protein levels of MMP2 and TIMP2 by ELISA we found only the MMP2 was significantly increased in the HHcy mice compared with control mice and TIMP2 was unchanged. With respect to the MMP9 system, we found that MMP3 and MMP9 gene expression levels were significantly increased in the HHcy mice compared with the control mice but the TIMP1 levels were unchanged (Figure 5C). Protein expression of MMP9 and TIMP1, measured by ELISA, showed the same pattern as the gene expression analysis (Figure 5D). Gelatin zymography provides measurement of MMP activity. Figure 5E shows a representative stained gel with the bands that were identified as pro-MMP9, active-MMP9, pro-MMP2, and active-MMP2 based on molecular weight as shown previously,[17] and western blot confirmation of molecular weights. Densitometry analysis of the bands of interest normalized to the BCA analysis of the protein loaded onto the gel showed that the active-MMP9 and active-MMP2 bands were significantly more intense for the HHcy mice than the control mice (Figure 5F).

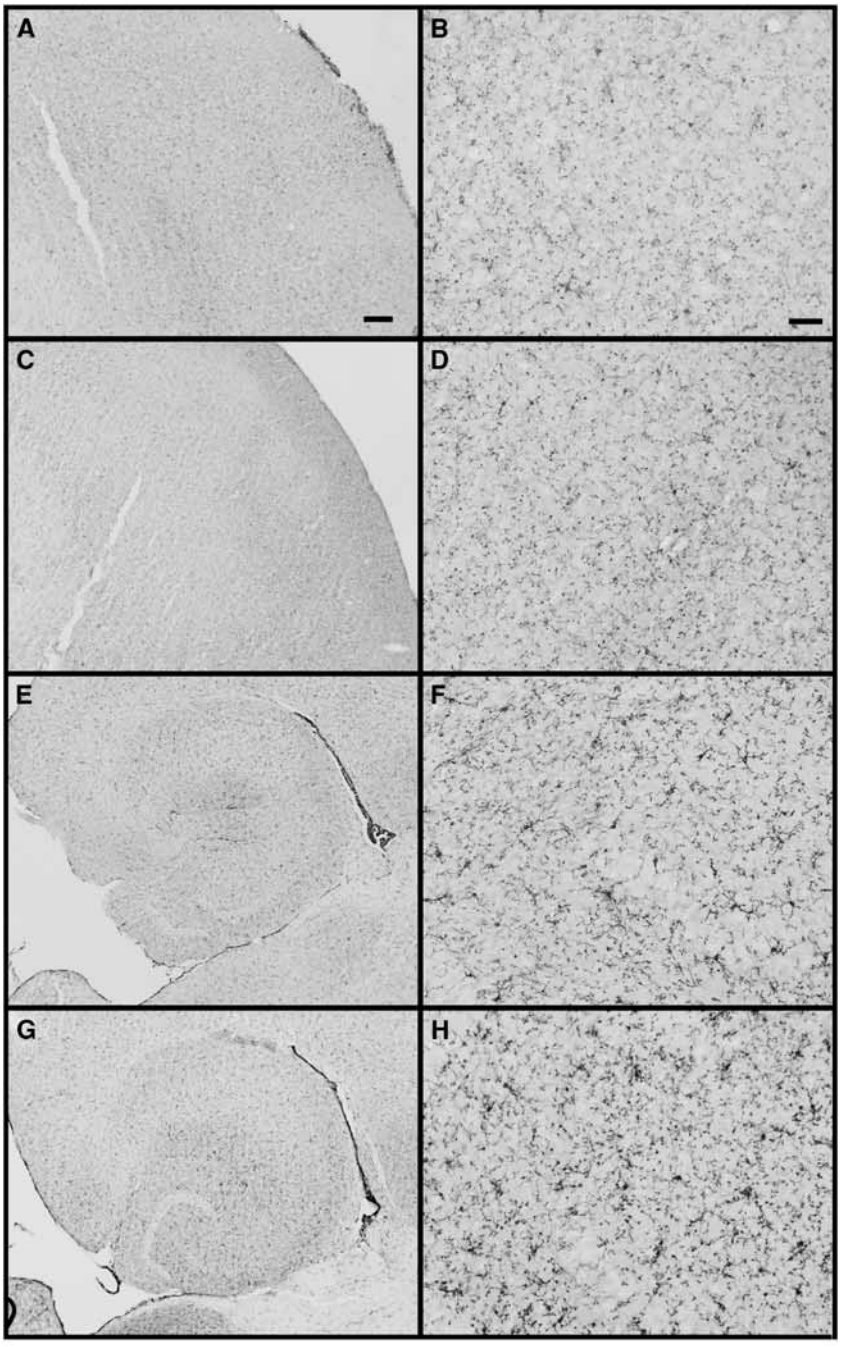

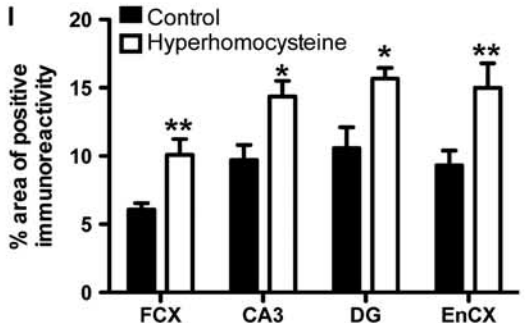

Figure 3. Hyperhomocysteinemia (HHCy) is associated with microglial activation. (**A**–**H**) CD11b immunohistochemistry in the frontal cortex (**A**–**D**) and hippocampus (**E**–**H**) of wild-type mice receiving control diet (**A**–**B** and **E**–**F**) or experimental diet (**C**–**D** and **G**–**H**) is shown. (**A**, **C**, **E**, **G**) Magnification = × 4, scale bar in (**A**) for (**A**), (**C**), (**E**), and (G) = 120 μm. (**B**, **D**, **F**, **H**) Magnification = × 200, scale bar in (**B**) for (**B**), (**D**), (**F**), and (**H**) = 25 μm. (**B**, **D**, **F**, **H**) High magnification images of (**A**), (**C**), (**E**), and (**G**), respectively. (**I**) Quantification of percent area occupied by positive stain for CD11b in the frontal cortex (FCX), CA3, and dentate gyrus (DG) of the hippocampus and the entorhinal cortex (EnCX). *Indicates $P < 0.05$ and **indicates $P < 0.01$ by *t*-test.

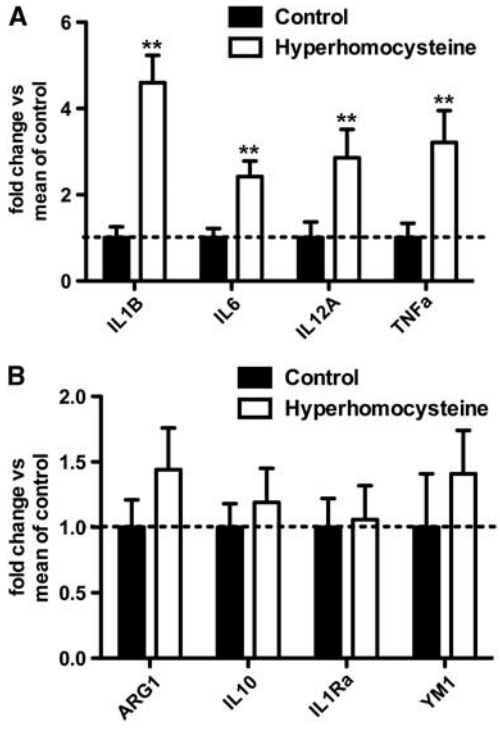

Figure 4. Phenotyping of neuroinflammation shows that hyperhomocysteinemia (HHCy) is associated with an M1, but not an M2, neuroinflammation in the brain. (**A**) Quantitative real-time RT-PCR analysis for M1 markers and (**B**) analysis of M2 markers are shown. **Indicates $P < 0.01$ by *t*-tests. Data are shown as fold change versus mean of control, where the mean of control indicates the mean of the mice on control diet for the given gene.

DISCUSSION

Vascular dementia is second only to AD as a cause of dementia. In addition, it is estimated that as many as 40% of AD patients actually have a mixed dementia, indicating that their dementia is caused not only by AD pathology but also by cerebrovascular pathology.[3] Despite the prevalence of VaD, the mouse models available to study VaD have been relatively lacking compared with those available for the study of AD pathology. Many models that have been studied involve acute, severe brain injuries such as embolism or arterial occlusion and typical cognitive testing that is reported in AD models has not been extensively performed.[18] Here, we report on a mouse model of VaD that develops multiple microhemorrhages, neuroinflammation, and cognitive impairment. We have achieved this model of VaD by dietary induction of HHcy in wild-type mice. Hyperhomocysteinemia has been clinically associated with cardiovascular disease,[19] cerebrovascular disease[20] and, recently, AD.[21]

Homocysteine is a nonprotein forming sulfur amino acid involved in methylation and transulfuration generated during 1-carbon metabolism. Elevated plasma levels of homocysteine, HHcy, can be achieved either genetically or through diet modification. Genetically, deletion of the cystathionine-β-synthase gene results in HHcy by altering the 1-carbon metabolic pathway.[22] Deletion of the methylenetetrahydrofolate reductase gene, a key component in the 1-carbon metabolic pathway, also results in severe HHcy in mice.[23] Dietary modification can either directly supplement homocysteine to the diet, and therefore increase plasma homocysteine levels,[9] or target the 1-carbon metabolic pathway to induce excessive production of homocysteine leading to HHcy.[8] We chose to pursue the targeting of the metabolic pathway. Our mouse diet is deficient in folate, B6, and B12 and is enriched with methionine.[8] These factors result in the overproduction of homocysteine in the 1-carbon metabolic pathway and result in HHcy. We found a moderate HHcy as assessed by terminal plasma collection based on the mouse criteria established by Ernest *et al*.[16]

While B-vitamin deficiency has been shown to result in cognitive impairment, in particular B12,[24] it is not clear whether this is a direct consequence of B12 deficiency or whether the cognitive impairment is a result of the subsequent HHCy. Vitamin B6 deficiency is associated with inflammation-associated diseases such as rheumatoid arthritis, irritable bowel disease, and coronary heart disease.[25] Again, it is difficult to discern direct effects of B-vitamin deficiency and effects of the resulting HHCy. The genetic models of HHCy help us to conclude that our findings are primarily related to the HHCy induced. A heterozygous cystathionine-β-synthase knockout mouse model of HHCy shows increased brain permeability with increased MMP9 and MMP2 activity.[26] Behavioral analysis on the genetic mouse models of HHCy is rare because of the severity of the phenotype, but studies in both genetic mouse models have shown behavioral deficits.[27,28] Because of the body of data related to B-vitamin deficiency, we cannot exclude the possibility that some of our findings are because of the dietary exclusion of these nutrients.

We found that HHcy was associated with significant impairment in the 2-day radial-arm water maze task. This is the same task that we have previously used to show spatial memory deficits in amyloid precursor protein transgenic mouse models of AD-like amyloid pathology,[11] as well as amyloid targeted therapeutic improvements.[12] To determine the cause of the cognitive impairment, we performed T2* MRI on a subset of our mice. We found a significant number of cerebrovascular abnormalities that gave the appearance of microhemorrhages similar to those seen in the studies of Luo *et al*[29] who showed that MRI could be used to assess the immunotherapeutic exacerbation of cerebral amyloid angiopathy-induced microhemorrhage. The MRI sequence we chose, the T2*, is the same sequence used by Luo and colleagues and also the same used in human studies of microhemorrhages.[30] Once brain tissue was harvested we performed Prussian blue staining on tissue sections to assess microhemorrhages histologically. We found that the Prussian blue staining detects a greater number of microhemorrhages than does the MRI; however, the MRI was able to provide the same diet effect and the same statistical significance of HHcy.

The direct consequence of microhemorrhages on cognition has remained elusive. There are many correlative studies in humans that have shown microhemorrhages contributing to cognitive impairment,[31] however, the majority of these have been in patients with other underlying neurologic disorders such as AD, stroke, transient ischemic attacks, or cerebral autosomal dominant arteriopathy with subcortical infarcts and leukoencephalopathy. Only the Yakushiji *et al*[32] study examined healthy adults and showed lower mini-mental state examination scores with the presence of microbleeds on MRI. Studies in mouse models that have shown microhemorrhages have been complicated by other pathologies. In anti-Aβ immunotherapy studies, the therapeutic benefit of the antibodies on cognition has far outweighed any potential adverse effect of the presence of microhemorrhages.[12] In cerebral amyloid angiopathy mouse models, it has not been possible to separate out the cognitive effects of the amyloid pathology from any cognitive effects of the microhemorrhages.

To address the mechanism by which HHcy results in microhemorrhages, we focused on the neuroinflammatory response and the subsequent activation of MMPs, since we did not observe significant changes in the clotting factors. We have previously shown that microhemorrhages because of anti-Aβ immunotherapy are associated with an enhanced M1-type neuroinflammatory response.[14] To characterize the inflammatory response, we have chosen to use the M1-M2 phenotype characterization used in the peripheral macrophage literature.[33]

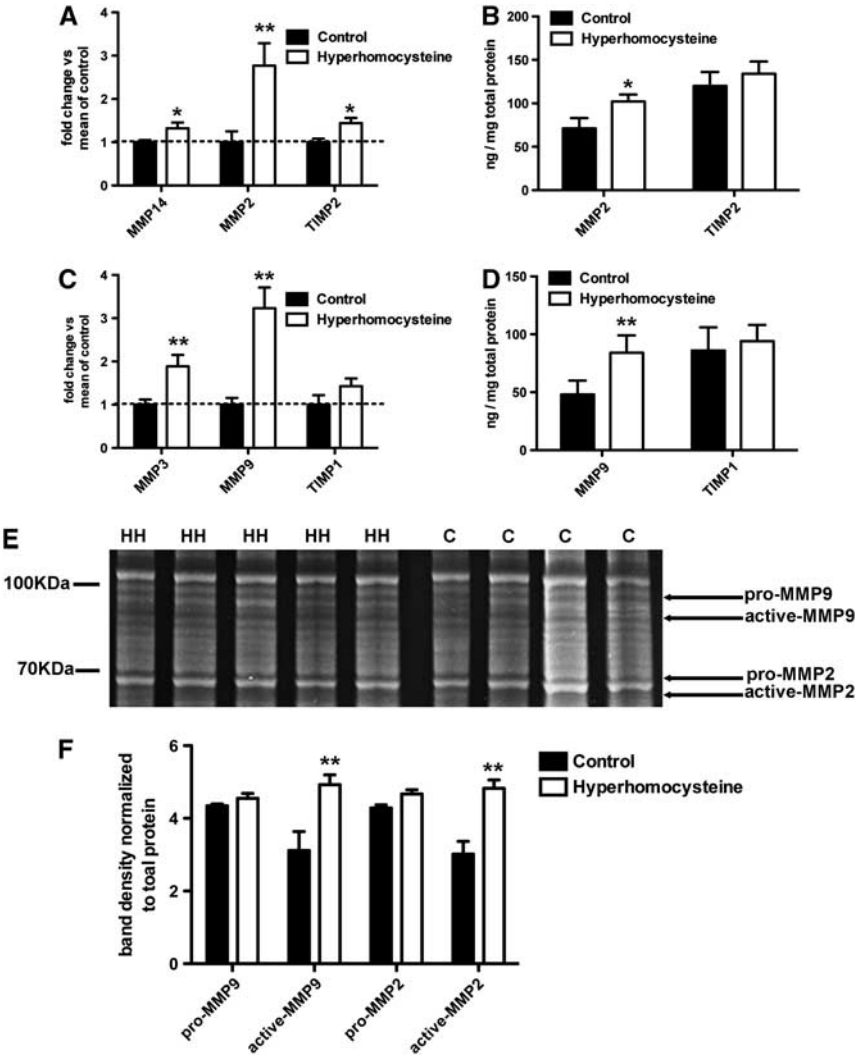

Figure 5. The matrix metalloproteinase 2 (MMP2) and MMP9 systems in the brain are activated by hyperhomocysteinemia (HHCy). (**A**, **C**) Quantitative real-time RT-PCR or MMP14, MMP2, and tissue inhibitor of metalloproteinase 2 (TIMP2) of the MMP2 system (**A**) and MMP3, MMP9, and TIMP1 of the MMP9 system (**C**) are shown. (**B**, **D**) ELISA data for MMP2 and TIMP2 of the MMP2 system (**B**) and MMP9 and TIMP1 of the MMP9 system (**D**) are shown. *Indicates $P<0.05$ and **indicates $P<0.01$ by *t*-tests. (**E**) A gelatin zymogram where HH indicates a sample from a hyperhomocysteinemic mouse and C indicates a sample from a control mouse. On the left of the image, for reference, shows where the molecular weight markers are. Shown on the right of the image are arrows indicating which bands are for the pro and active forms of MMP2 and MMP9 based on their molecular weight. Pro-MMP9 is 92 kDa and active MMP9 is 82 kDa. Pro-MMP2 is 70 to 72 kDa and active MMP2 is 62 to 65 kDa. (**F**) Densitometry analysis of the digested bands on the zymogram normalized to the absolute amount of protein loaded onto the gel is shown. **Indicates $P<0.01$ by *t*-tests.

M1 describes a classic inflammatory response characterized by the expression of IL-1β, TNFα, IL-6, and IL-12, while M2 responses are more closely associated with an alternative inflammatory response that is characterized by the expression of wound repair and anti-inflammatory genes like arginase 1, YM1, IL-1 receptor antagonist, and IL-10.[34] We found that there was increased microglial activation in our HHcy mice, as evidenced by increased CD11b immunostaining. In addition, we found that the neuroinflammatory response in the HHcy mice was primarily an M1 response, with significantly increased expression of M1 genes but no increase in expression of M2 genes. It is possible that this exacerbated M1-type neuroinflammation contributes significantly to the cognitive deficits in the HHCy mice. IL-1β, TNFα, and IL-6 have all been shown to independently result in cognitive impairment.[35–37] We hypothesize that the significant induction of M1 neuroinflammation contributes to the cognitive impairment in the HHCy mice.

Matrix metalloproteinases, in particular MMP2 and MMP9, are heavily implicated in the pathogenesis of hemorrhagic events, both systemically and in the brain.[38,39] We have previously shown that the MMP2 and MMP9 systems are activated after anti-Aβ immunotherapy treatment in amyloid precursor protein transgenic mice where microhemorrhage was observed as an adverse event.[17] Others have identified MMP9 as a cause of cerebral amyloid angiopathy-associated hemorrhages.[40] We found that our HHcy had significantly increased expression of MMP2 and MMP9 at both the RNA and protein level. In addition, both MMP14, the activator of MMP2, and MMP3, the activator of MMP9, were increased in their gene expression. Protein expression of the endogenous inhibitors of MMP2 and MMP9, TIMP2 and TIMP1, respectively, was not significantly altered by HHcy. When we performed gelatin zymography on fresh brain tissue we found that HHcy also increased the activity of active MMP2 and active MMP9, indicating that the increased expression of

these proteins had resulted in a functional increase in the activity of the enzymes.

In summary, we have found that HHcy is associated with induction of an M1 neuroinflammation, activation of MMP2 and MMP9, cerebrovascular microhemorrhages and learning and memory deficits. We believe that this represents a unique mouse model of VaD that can be used to study therapeutic approaches to treat VaD, molecular mechanisms of VaD, and comorbidities of VaD with other forms of dementia such as AD.

DISCLOSURE/CONFLICT OF INTEREST

The authors declare no conflict of interest.

REFERENCES

1 Roman GC. Vascular dementia revisited: diagnosis, pathogenesis, treatment, and prevention. *Med Clin North Am* 2002; **86**: 477–499.
2 Dubois MF, Hebert R. The incidence of vascular dementia in Canada: a comparison with Europe and East Asia. *Neuroepidemiology* 2001; **20**: 179–187.
3 Kammoun S, Gold G, Bouras C, Giannakopoulos P, McGee W, Herrmann F *et al.* Immediate causes of death of demented and non-demented elderly. *Acta Neurol Scand Suppl* 2000; **176**: 96–99.
4 Schneider JA, Arvanitakis Z, Leurgans SE, Bennett DA. The neuropathology of probable Alzheimer disease and mild cognitive impairment. *Ann Neurol* 2009; **66**: 200–208.
5 Gorelick PB, Scuteri A, Black SE, Decarli C, Greenberg SM, Iadecola C *et al.* Vascular contributions to cognitive impairment and dementia: a statement for healthcare professionals from the American Heart Association/American Stroke Association. *Stroke* 2011; **42**: 2672–2713.
6 Mudd SH, Finkelstein JD, Irreverre F, Laster L. Homocystinuria: an enzymatic defect. *Science* 1964; **143**: 1443–1445.
7 Troen AM, Shea-Budgell M, Shukitt-Hale B, Smith DE, Selhub J, Rosenberg IH. B-vitamin deficiency causes hyperhomocysteinemia and vascular cognitive impairment in mice. *Proc Natl Acad Sci USA* 2008; **105**: 12474–12479.
8 Hofmann MA, Lalla E, Lu Y, Gleason MR, Wolf BM, Tanji N *et al.* Hyperhomocysteinemia enhances vascular inflammation and accelerates atherosclerosis in a murine model. *J Clin Invest* 2001; **107**: 675–683.
9 Pirchl M, Ullrich C, Humpel C. Differential effects of short- and long-term hyperhomocysteinaemia on cholinergic neurons, spatial memory and microbleedings in vivo in rats. *Eur J Neurosci* 2010; **32**: 1516–1527.
10 Alamed J, Wilcock DM, Diamond DM, Gordon MN, Morgan D. Two-day radial-arm water maze learning and memory task; robust resolution of amyloid-related memory deficits in transgenic mice. *Nat Protoc* 2006; **1**: 1671–1679.
11 Wilcock DM, Lewis MR, Van Nostrand WE, Davis J, Previti ML, Gharkholonarehe N *et al.* Progression of amyloid pathology to Alzheimer's disease pathology in an amyloid precursor protein transgenic mouse model by removal of nitric oxide synthase 2. *J Neurosci* 2008; **28**: 1537–1545.
12 Wilcock DM, Rojiani A, Rosenthal A, Subbarao S, Freeman MJ, Gordon MN *et al.* Passive immunotherapy against Abeta in aged APP-transgenic mice reverses cognitive deficits and depletes parenchymal amyloid deposits in spite of increased vascular amyloid and microhemorrhage. *J Neuroinflammation* 2004; **1**: 24.
13 Sudduth TL, Wilson JG, Everhart A, Colton CA, Wilcock DM. Lithium treatment of APPSwDI/NOS2 $-/-$ mice leads to reduced hyperphosphorylated tau, increased amyloid deposition and altered inflammatory phenotype. *PLoS ONE* 2012; **7**: e31993.
14 Wilcock DM, Zhao Q, Morgan D, Gordon MN, Everhart A, Wilson JG *et al.* Diverse inflammatory responses in transgenic mouse models of AD and the effect of immunotherapy on these responses. *ASN neuro* 2011; **3**: 249–258.
15 Livak KJ, Schmittgen TD. Analysis of relative gene expression data using real-time quantitative PCR and the 2(-Delta Delta C(T)) Method. *Methods* 2001; **25**: 402–408.
16 Ernest S, Hosack A, O'Brien WE, Rosenblatt DS, Nadeau JH. Homocysteine levels in A/J and C57BL/6J mice: genetic, diet, gender, and parental effects. *Physiol Genomics* 2005; **21**: 404–410.
17 Wilcock DM, Morgan D, Gordon MN, Taylor TL, Ridnour LA, Wink DA *et al.* Activation of matrix metalloproteinases following anti-Abeta immunotherapy; implications for microhemorrhage occurrence. *J Neuroinflammation* 2011; **8**: 115.
18 Jiwa NS, Garrard P, Hainsworth AH. Experimental models of vascular dementia and vascular cognitive impairment: a systematic review. *J Neurochem* 2010; **115**: 814–828.
19 Eikelboom JW, Lonn E, Genest Jr J, Hankey G, Yusuf S. Homocyst(e)ine and cardiovascular disease: a critical review of the epidemiologic evidence. *Ann Intern Med* 1999; **131**: 363–375.
20 Bostom AG, Rosenberg IH, Silbershatz H, Jacques PF, Selhub J, D'Agostino RB *et al.* Nonfasting plasma total homocysteine levels and stroke incidence in elderly persons: the Framingham Study. *Ann Intern Med* 1999; **131**: 352–355.
21 Van Dam F, Van Gool WA. Hyperhomocysteinemia and Alzheimer's disease: a systematic review. *Arch Gerontol Geriatr* 2009; **48**: 425–430.
22 Lentz SR, Erger RA, Dayal S, Maeda N, Malinow MR, Heistad DD *et al.* Folate dependence of hyperhomocysteinemia and vascular dysfunction in cystathionine beta-synthase-deficient mice. *Am J Physiol Heart Circ Physiol* 2000; **279**: H970–H975.
23 Chen Z, Karaplis AC, Ackerman SL, Pogribny IP, Melnyk S, Lussier-Cacan S *et al.* Mice deficient in methylenetetrahydrofolate reductase exhibit hyperhomocysteinemia and decreased methylation capacity, with neuropathology and aortic lipid deposition. *Hum Mol Genet* 2001; **10**: 433–443.
24 Moore E, Mander A, Ames D, Carne R, Sanders K, Watters D. Cognitive impairment and vitamin B12: a review. *Int Psychogeriatr* 2012; **24**: 541–556.
25 Lotto V, Choi SW, Friso S. Vitamin B6: a challenging link between nutrition and inflammation in CVD. *Br J Nutr* 2011; **106**: 183–195.
26 Kumar M, Tyagi N, Moshal KS, Sen U, Kundu S, Mishra PK *et al.* Homocysteine decreases blood flow to the brain due to vascular resistance in carotid artery. *Neurochem Int* 2008; **53**: 214–219.
27 Akahoshi N, Kobayashi C, Ishizaki Y, Izumi T, Himi T, Suematsu M *et al.* Genetic background conversion ameliorates semi-lethality and permits behavioral analyses in cystathionine beta-synthase-deficient mice, an animal model for hyperhomocysteinemia. *Hum Mol Genet* 2008; **17**: 1994–2005.
28 Jadavji NM, Deng L, Leclerc D, Malysheva O, Bedell BJ, Caudill MA *et al.* Severe methylenetetrahydrofolate reductase deficiency in mice results in behavioral anomalies with morphological and biochemical changes in hippocampus. *Mol Genet Metab* 2012; **106**: 149–159.
29 Luo F, Rustay NR, Seifert T, Roesner B, Hradil V, Hillen H *et al.* Magnetic resonance imaging detection and time course of cerebral microhemorrhages during passive immunotherapy in living amyloid precursor protein transgenic mice. *J Pharmacol Exp Ther* 2010; **335**: 580–588.
30 Sperling RA, Jack Jr CR, Black SE, Frosch MP, Greenberg SM, Hyman BT *et al.* Amyloid-related imaging abnormalities in amyloid-modifying therapeutic trials: recommendations from the Alzheimer's Association Research Roundtable Workgroup. *Alzheimers Dement* 2011; **7**: 367–385.
31 Goos JD, Henneman WJ, Sluimer JD, Vrenken H, Sluimer IC, Barkhof F *et al.* Incidence of cerebral microbleeds: a longitudinal study in a memory clinic population. *Neurology* 2010; **74**: 1954–1960.
32 Yakushiji Y, Nishiyama M, Yakushiji S, Hirotsu T, Uchino A, Nakajima J *et al.* Brain microbleeds and global cognitive function in adults without neurological disorder. *Stroke* 2008; **39**: 3323–3328.
33 Mosser DM, Edwards JP. Exploring the full spectrum of macrophage activation. *Nat Rev Immunol* 2008; **8**: 958–969.
34 Wilcock DMA. Changing perspective on the role of neuroinflammation in Alzheimer's disease. *Int J Alzheimers Dis* 2012; **2012**: 495243.
35 Kitazawa M, Cheng D, Tsukamoto MR, Koike MA, Wes PD, Vasilevko V *et al.* Blocking IL-1 signaling rescues cognition, attenuates tau pathology, and restores neuronal beta-catenin pathway function in an Alzheimer's disease model. *J Immunol* 2011; **187**: 6539–6549.
36 Dugan LL, Ali SS, Shekhtman G, Roberts AJ, Lucero J, Quick KL *et al.* IL-6 mediated degeneration of forebrain GABAergic interneurons and cognitive impairment in aged mice through activation of neuronal NADPH oxidase. *PLoS ONE* 2009; **4**: e5518.
37 Belarbi K, Jopson T, Tweedie D, Arellano C, Luo W, Greig NH *et al.* TNF-alpha protein synthesis inhibitor restores neuronal function and reverses cognitive deficits induced by chronic neuroinflammation. *J Neuroinflammation* 2012; **9**: 23.
38 Klein T, Bischoff R. Physiology and pathophysiology of matrix metalloproteases. *Amino Acids* 2011; **41**: 271–290.
39 Candelario-Jalil E, Thompson J, Taheri S, Grossetete M, Adair JC, Edmonds E *et al.* Matrix metalloproteinases are associated with increased blood-brain barrier opening in vascular cognitive impairment. *Stroke* 2011; **42**: 1345–1350.
40 Hernandez-Guillamon M, Martinez-Saez E, Delgado P, Domingues-Montanari S, Boada C, Penalba A *et al.* MMP-2/MMP-9 plasma level and brain expression in cerebral amyloid angiopathy-associated hemorrhagic stroke. *Brain Pathol* 2011; **22**: 133–141.

Supplementary Information accompanies this paper on the Journal of Cerebral Blood Flow & Metabolism website (http://www.nature.com/jcbfm)